Microplastics and Nanoplastics

RESEARCH

Open Access

# Mobility and retention of microplastic fibers and irregular plastic fragments in fluvial systems: an experimental flume study

Marco La Capra[1*], Daniel Wagner[2], Seema Agarwal[2], Jan H. Fleckenstein[3,4] and Sven Frei[5]

**Abstract**

Pore-scale microplastics (< 10 µm) are emerging contaminants whose behavior and fate in aquatic environments remain poorly understood. While the transport and retention of spherical microplastics (SMPs) have been studied in fluvial systems, irregularly shaped microplastics (IMPs) and microplastic fibers (MPFs) remain poorly understood. This study investigates how IMPs and MPFs differ from SMPs in their transport and retention in open stream and hyporheic flows under controlled flume conditions using fluorescently labeled particles. We compared the transport dynamics of IMPs (d90 = 7.68 µm) and MPFs (diameter 5–10 µm, length 60–250 µm) with reference SMPs (1, 3, and 10 µm in diameter) by continuously monitoring microplastic concentrations in surface water and streambed sediments. IMPs exhibited mobility similar to SMPs, with minor retention in the system. In contrast, MPFs showed markedly higher retention, preferentially accumulating at the sediment–water interface, where ~9% of the introduced mass was retained. These findings demonstrate that particle shape and aspect ratio strongly influence microplastic transport and retention in fluvial systems, with implications for their ecological impacts and long-term fate.

**Keywords** Microplastic transport, Hyporheic zone, Microplastic retention, Microplastic shape, Fluorescence imaging, Freshwater pollution

*Correspondence:
Marco La Capra
Marco.La-Capra@uni-bayreuth.de

Full list of author information is available at the end of the article

**Graphical Abstract**

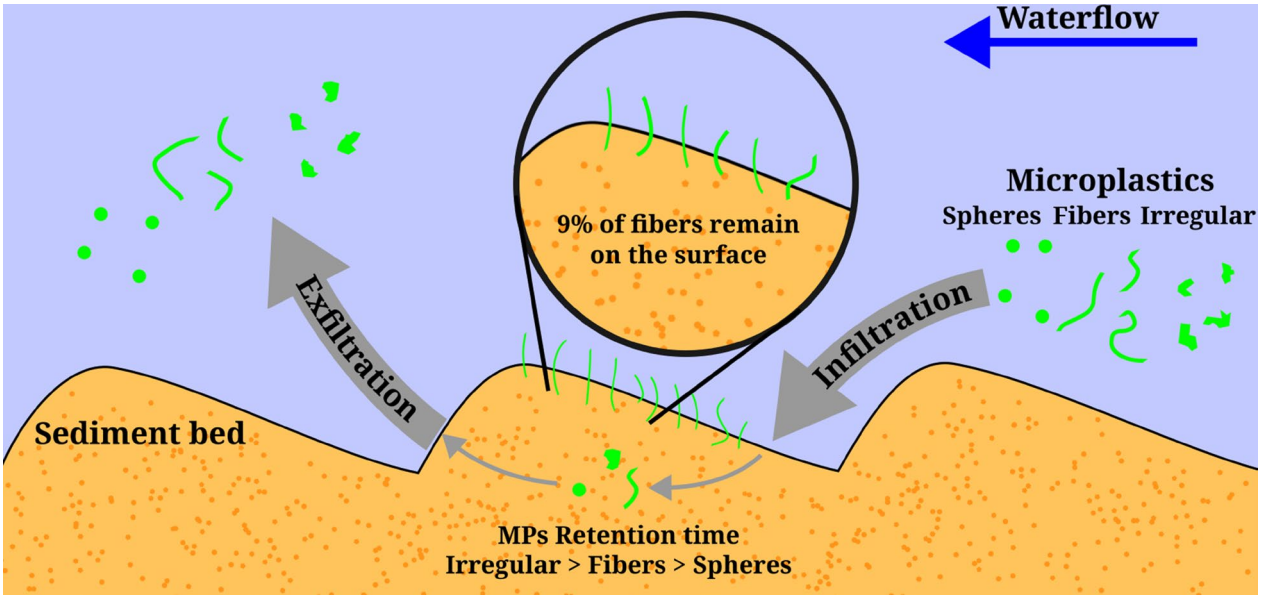


## Introduction

Microplastics (MPs) are pervasive contaminants that have seen an increased interest from the scientific community since the early 2000s [1]. MPs have been identified by the UN as one of six emerging environmental issues [2] and occur ubiquitously across multiple components of ecosystems. High concentrations of MPs have been reported in the hydrosphere [3–5], the lithosphere [3, 6], and even in remote environments such as the Mariana Trench [7]. Importantly, these particles have been shown to have adverse effects in areas where high concentrations were found. In contaminated soils, MPs have been shown to alter biophysical soil properties [8] and disrupt soil biota [9]. Moreover, MPs have been linked to potential toxicological effects [10]. Risks posed by MPs to human health arise from exposure through drinking water [11] and food consumption [12]. Although the implications of MPs' exposure remain uncertain, their widespread presence underscores the need for further research.

Once released into the environment, understanding the behavior of MPs is crucial for assessing their potential hazardous effects and determining exposure timescales across different ecosystem compartments. Occurrence and behavior of MPs in freshwater and marine systems have been widely studied [13, 14], including their infiltration behavior into streambed, lake, and marine sediments [15–17]. While rivers and streams serve as major transport vectors for MPs entering marine environments [18], streambed sediments have been identified to act as preferential net sinks for different types of MPs. This manifests with MPs being retained within the sediment of MP-laden streams [19, 20]. Depending on the polymer type, MPs can be transported primarily either at the water surface, suspended within the water column, or can accumulate in streambed sediments [21, 22]. However, it has also been reported that particle density is not fixed in natural systems; it can be altered by various environmental processes such as biofouling, aggregation with organic matter, or degradation [23–25]. These processes can cause originally buoyant particles to become non-buoyant and vice versa, changing their transport behavior. Furthermore, the transport mechanisms of MPs have been shown to be impacted by their shape. Fibers were found to deposit more slowly than fragments in settling column experiments [26]. In turbidity currents, fibers are more preferentially buried within the sand deposits, while fragments are carried by the current [27, 28]. Sedimentation and resuspension cycles of MPs in fluvial systems are highly dynamic and influenced by hydrological forcing and streambed characteristics. High loads of resuspended MPs have been observed during flood events, with significant fractions of previously deposited particles being mobilized from streambed sediments [29]. Given the complexity and variability of MPs transport in these environments, a thorough understanding of their transport behavior, interactions with the water–sediment interface, and mobility within streambed sediments is essential.

MPs commonly found in the environment exhibit considerable variability in material, size, and shape [30]. These heterogeneous characteristics influence both their environmental behavior and their potential ecological impacts [31]. Historically, many process-based and

empirical frameworks developed for sediment transport have been applied to describe MP behavior, despite evidence that MPs differ fundamentally from mineral particles in their transport dynamics [32]. Research has shown that larger spherical MPs (SMPs, typically greater than 100 µm) are generally unable to advectively pass the water-sediment interface of streambed sediments commonly found in rivers and streams [33]. In contrast, smaller pore-scale MPs (< 10 µm) were reported in laboratory and modelling experiments to penetrate the streambed easily due to advection and exhibit a high mobility within them [34, 35].

Despite the mechanistic insights provided by flume and column experiments [32, 34], our understanding of how the form and shape of MPs influence their transfer from surface flow into streambed sediments, as well as their mobility within these sediments, remains limited. To date, experiments under realistic conditions have mainly been performed using spherical microplastics [34, 36]. However, previous studies have shown that spherical particles often represent only a minority within streambed sediments [19]. In contrast, microplastic fibers (MPFs) and irregularly shaped particles (IMPs) have been found in substantially higher quantities in many fluvial systems [37–39].

To improve our understanding of the mobility and retention of MPFs and IMPs in streambed sediments in comparison to SMPs, we performed flume experiments under conditions that replicated realistic hydraulic flow conditions in streams and sediment. Building on the experimental setup of Boos et al. [34], we investigated the infiltration behavior of pore-scale MPFs and IMPs. Using a fluorescence imaging system and continuously operating fluorometers, we were able to track the movement of MPFs and IMPs across (1) the surface flow (2), the streambed-water interface, and (3) within the streambed sediments. To contextualize our findings, we compared the transport behavior of MPFs and IMPs to that of a nearly conservative solute (fluorescein) and SMPs of similar sizes. The objectives of the experimental setup were threefold: (1) To compare the mobility of MPFs and IMPs with that of SMPs and a conservative solute (2), To assess the infiltration dynamics and penetration depths of MPFs and IMPs into streambed sediments, thereby improving our understanding of their mobility and exposure timescales, and (3) to evaluate the extent of retention of MPFs and IMPs within the streambed sediments.

## Materials and methods

### Experimental flume setup

Experiments were performed in a closed-circuit experimental flume (*HM 160 Experimental flume 86 × 300, G.U.N.T. Gerätebau GmbH equipped with HM 160.10 Extension element, G.U.N.T. Gerätebau GmbH*) using deionized (DI) water. DI water was used to minimize the variability in the water contents between experiments, to reduce the background of the measurement instruments, and to keep organic matter to a minimum. Discharge in the flume was kept as close to 1 $m^3\ h^{-1}$ (0.278 $L\ s^{-1}$) as possible using an electropneumatic valve (*GF Ltd.*) and was monitored with an electromagnetic flow meter (*Jumo GmbH*). This discharge resulted in an average stream velocity of 0.1 $m\ s^{-1}$. Three weirs of the same height were positioned at x = 0.00 m, x = 2.40 m, and x = 4.90 m. This was done to ensure a constant water height throughout the flume. The section of the flume between the weirs at x = 4.90 m and x = 2.40 m was filled with $d_{50}$ = 1.0 mm unimodal sand. Such sand was used to represent commonly found sediments in streams and was formed according to the 2D geometry of commonly found sediment ripples in streams [40]. We formed these ripples to be 20 cm long and 5 cm high, with their stoss and lee sides measuring 15 cm and 5 cm, respectively. We chose this ripple size to ensure the field of view of our instruments encompasses the entirety of the ripple. We placed a temperature sensor (*Onset HOBO TidbiT v2, LI-COR Environmental*) before the weir at x = 0.00 m, and six ultrasonic sensors (*UFP-200, WayCon Positionsmesstechnik GmbH*) on top of the flume between x = 4.90 m and x = 2.40 m weir. An infrared laser (*MLSL226, wenglor*) was placed on top of the weir at x = 2.40 m to measure the evolution of the sediment profile during the experiment. The laser was also used to measure the complete sediment profile at the end of the experiment (Fig. 1). The MPs' suspensions were injected at position x = 0.00 m, and data were recorded for 30 min after the injection. While the glass walls might influence the transport within a flume of the dimensions such as the one we used, such effects were assessed by Dichganz et al. [35]. The difference between the concentration at the glass wall and that at the center of the flume was found to be minimal. As such, we consider the influence of the flume wall to be negligible. The outflowing water was collected during the experiment, and DI water was continuously pumped into the flume. A PIV system was used to monitor surface flow characteristics during the experiments using a system consisting of an LED line emitter (iLA.LPS 3, iLA-5150), a CMOS camera (PIV. Nano, iLA-5150), and a synchroniser (Synchroniser, iLA-5150). The light was affixed to the top of the flume walls, with the LED light sheet parallel to the glass walls and the camera perpendicular to the wall. Measurements were taken along the study area.

### Microplastic particles and fluorescein

The MPFs and the IMPs were produced at the University of Bayreuth (Chair of Macromolecular Chemistry I). For easier detection, the MPFs were labelled with Fluorescein. To prevent the leaching of Fluorescein into the

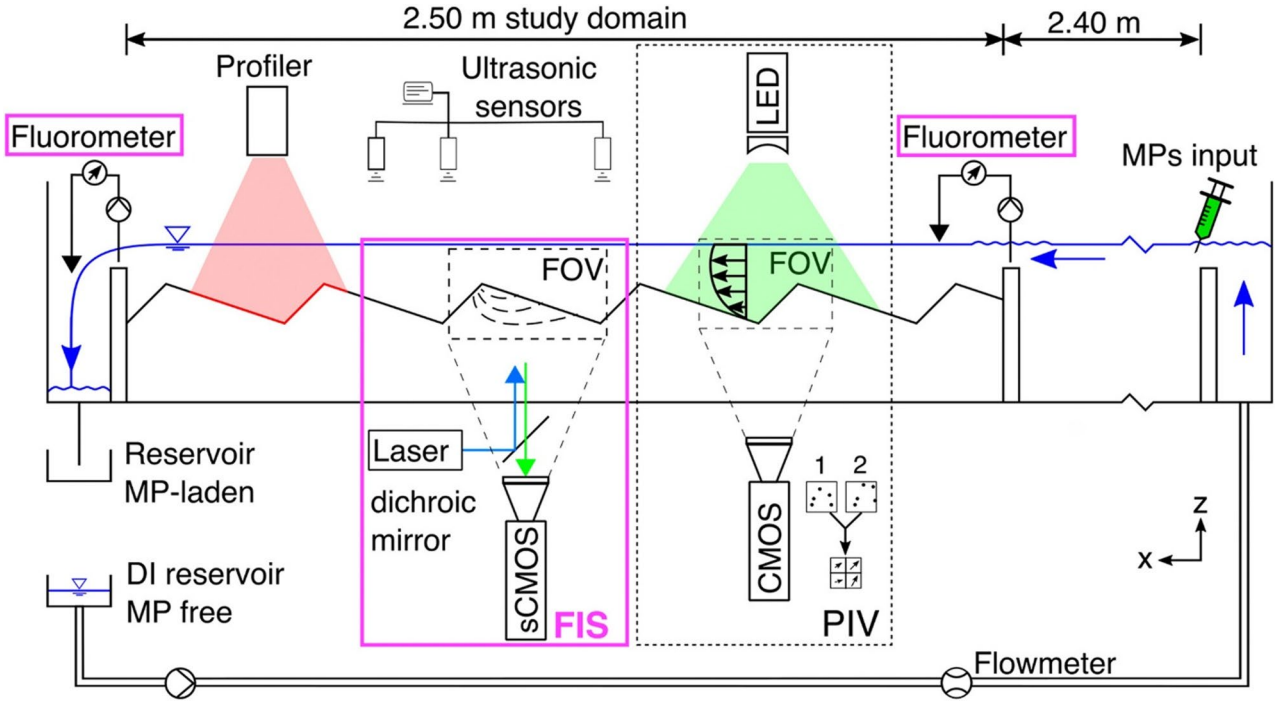


**Fig. 1** Schematic setup of the experimental flume adapted from Boos et al. [41]. The FIS and PIV analyses were conducted on top of the same sediment structure

water, the dye was covalently attached directly to the backbone of the polymer. This was achieved by radical copolymerization of styrene and fluorescein-O-methacrylate with AIBN as initiator. The content of dye was determined by 3.5% via NMR after synthesis. Detailed synthesis procedure and analysis are described in the SI. The production of fibers was done by electrospinning, since electrospinning was determined to be the best method to produce thin fibers at a laboratory scale [42]. To do so, 30 wt% of a 7:3 weight mixture of pure PS (*PS 158 N*, *Ineos Styrolution*, *Frankfurt am Main*, *Germany*) and PS-fluorescein labelled polymer was dissolved in dimethylformamide. This solution was filled in a plastic syringe (*Injekt*, *5 mL*) assembled with a blunt-ended stainless steel needle (Sterican, Ø = 0.8 mm) and connected to a high voltage source. The following conditions were applied for electrospinning: voltage 18 kV, flow rate 2 mL/h, and a distance between needle and collector of 15 cm. The electrospun nonwoven was collected on a flat plate collector covered by slick parchment paper connected to − 3 kV negative voltage. The electrospun nonwoven was cut into short fibers by a *Gastroback* kitchen mixer using water as a cutting medium [43, 44]. The rest of the water was removed by filtration using a PET mesh filter. The short fibers were dried by freeze-drying (*Christ Beta-2-16*). SEM images determined the sizes of the fibers and show a diameter of 5–10 µm and a length of 60–250 µm (Fig. 2).

The IMPs were produced by wet milling industrially produced fluorescent polyethylene MPs (*Cospheric*, *LLC*) to a $d_{90}$ = 7.68 µm (Table 1). For the wet milling, 4.8 g of Cospheric particles (53–63 µm) were suspended in 400 g of Milli-Q water and 1 g of the surfactant Triton X305 to prevent agglomeration. The particles were milled down in a Netzsch MiniCer (*Netzsch*, *Selb*, *Germany*) wet mill within 360 min using 489 g of 1.3 mm zeta beads as grinding body and a speed of 3000 rpm.

All particles were stored under dark conditions and at 4 °C to reduce the photochemical degradation of the fluorescent dye. Calibration suspensions were prepared using TWEEN20® (*CAS:9005-64-5*, *Sigma-Aldrich*) as a surfactant to keep the IMPs and MPFs in suspension. We used 220 mg $L^{-1}$ solutions of TWEEN20® for both IMPs and MPFs. Before their usage, we bathed the MPFs' suspensions in an ultrasound bath to untangle the fibers and minimize microplastic aggregates.

A fluorescein solution was prepared by dissolving fluorescein salt (*CAS No. 2321-07-5*, *Sigma-Aldrich*) in DI water and by diluting this solution to suit our experimental steps. This solution was kept at 4 °C and in the dark to avoid photochemical degradation. Fluorescein was used to assess the difference in behavior between a conservative solute and MPs.

At the end of each experiment, we cleaned the walls of the flume of any remaining MPs, and the sediment used was thoroughly washed with water to remove any leftover MPs. The water used for the experiment and

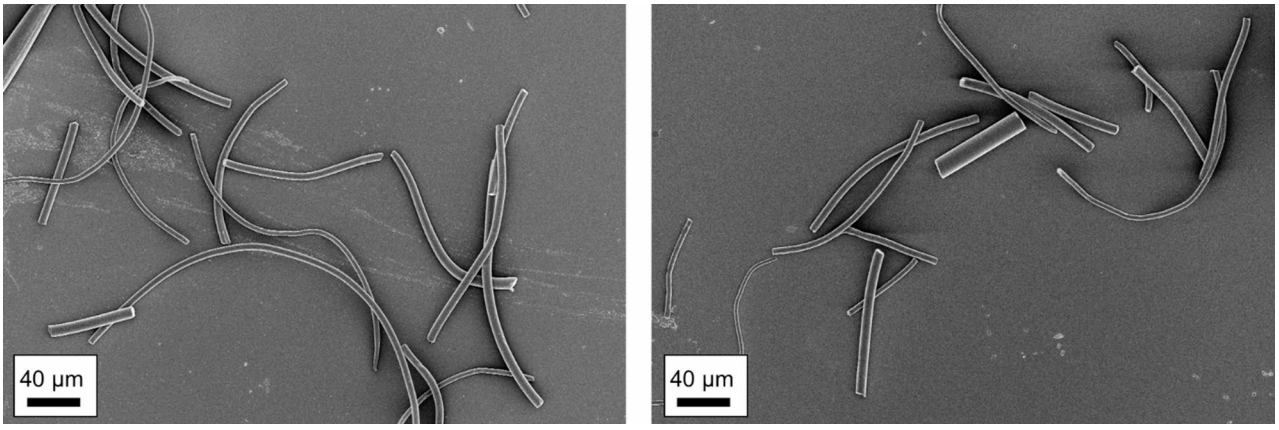


**Fig. 2** Morphology of PS-fluorescein labeled polymer short fibers. Images were taken using a scanning electron microscope (SEM, LEO 1530, Zeiss). The samples were first sputter-coated with Pt by a sputter coater with a Pt thickness of 2.5 nm (208 HR from Cressington, Watford, England)

**Table 1** $d_{MPs}$ refers to the diameter of the MPs (Note that for the IMPs, the d90 is given, and for the MPFs, the maximum and minimum of both diameter and length of the fiber are shown separately), $d_S$ refers to the mean sediment diameter, D refers to the MPs/sediment diameter ratio calculated as $\frac{d_{MPs}}{d_S}$ - Q refers to the mean discharge, and $m_0$ refers to the input particle mass. The IMPs are shown as for their particle size distribution. The particle size distribution was obtained by laser diffraction analysis (*Microtrac FlowSync*)

| ID | $d_{MPs}$ [µm] | $d_S$ [µm] | D [-] | Q [$m^3h^{-1}$] | $m_0$ [mg] |
|---|---|---|---|---|---|
| 1 µm SMPs | 1 | 1032 | 0.0010 | 1.09 | 54 |
| 3 µm SMPs | 3 | 1032 | 0.0029 | 1.09 | 98 |
| 10 µm SMPs | 10 | 1032 | 0.0097 | 1.00 | 78 |
| IMPs ($d_{10}$) | 4.15 | 1032 | 0.0040 | 1.02 | 802 |
| IMPs ($d_{50}$) | 5.15 | 1032 | 0.0050 | 1.02 | 802 |
| IMPs ($d_{90}$) | 7.68 | 1032 | 0.0072 | 1.02 | 802 |
| MPFs (min diameter) | 5 | 1032 | 0.0048 | 1.01 | 502 |
| MPFs (max diameter) | 10 | 1032 | 0.0097 | 1.01 | 502 |
| MPFs (min length) | 60 | 1032 | 0.0581 | 1.01 | 502 |
| MPFs (max length) | 250 | 1032 | 0.2422 | 1.01 | 502 |

the cleanup process was collected and filtered through two membrane filters, the first with a mesh of 0.45 µm and the second with a mesh of 0.04 µm (*Fuhr GmbH)*, to minimize the release of MPs into the sewer system. A summary of the characteristics of the experiments can be found in Table 1.

## Quantification and detection of fluorescent compounds

### *Surface water monitoring*

We used two portable fluorometers (*FL24, Albillia Co.*) to monitor fluorescein and the different MPs continuously. These fluorometers were produced based on Schnegg's design [45]. Water was pumped from the flume in the fluorometers using peristaltic pumps. Loss in the pump tubing was minimized by using tubes with a polished inner wall (Tygon® E-3603, *Saint-Gobain ICS*). This was done to reduce the outside effects of obstacles within the water flow. The fluorometers' inlet tubes were positioned at x = 2.40 m (inflow) and x = 4.90 m (outflow), on top of the weir's contouring the study area. Each MP type was calibrated individually to assess its response to the fluorometers. At least 30 measurements were averaged for each calibration concentration to reduce outliers. The limit of detection (LOD) and limit of quantification (LOQ) were then calculated from the calibration curves as $LOD = 3.3 \cdot \frac{\sigma}{m}$ and $LOQ = 10 \cdot \frac{\sigma}{m}$,

where σ is the standard deviation of the calibration curve, and m is the slope of the calibration curve. To allow for the comparison between experiments, a normalized mass transfer (NMT) was calculated as:

$$m\,(t) = \frac{c\,(t) \cdot Q\,(t)}{m_0} \left[T^{-1}\right], \tag{1}$$

where m(t) [-] is the normalized mass transfer at time t [T], c(t) [M/T] is the measured concentration at time t, Q(t) [$L^3$/T] is the measured discharge at time t, and $m_0$ [M] is the injected mass of the particles/fluorescent compound.

To analyze the MPs mass in the study area, the percentage of MPs captured by the streambed sediment was calculated as:

$$Q\,m\,(t) = \frac{(m_0 - \int_0^t m_{out} dt)}{m_0} \cdot 100 \tag{2}$$

Where Q m(t) [-] is the percentage ratio between introduced fluorescent compound mass and measured outflowing MPs mass at time t, $m_0$ is the injected mass of

MPs, and the integral represents the total mass measured at the outflow fluorometer for the time interval 0-t.

### *Fluorescent imaging system setup*

The Fluorescent Imaging System (FIS) has been described previously in Boos et al. [34]. We monitored MPs concentration in the streambed sediments by recording the glass interface of the flume with a scientific complementary metal-oxide-semiconductor (sCMOS) camera (*Prime BSI Express*, *Teledyne Vision Solutions*). This camera was outfitted with a camera objective (*f/0.95*, *50 mm focal length*). The fluorescein dye was excited using a 457 nm 100 mW laser (Cobolt 06-MLD 457 nm 100 W laser, Hübner Photonics), which was expanded using a 40x beam expander (*TSI Incorporated*). A dichroic mirror (*T470lpxr*, *Chroma Technology Corp.*) was placed at 45° in front of the camera objective. By doing so, the wavelength of the laser was reflected onto the study area of the flume. In contrast, the fluorescent light wavelength of the MPs and fluorescein could pass through the mirror (Fig. 3). This allowed us to investigate the concentration of the injected fluorescent compounds within the streambed sediments by detecting emitted fluorescent signals from the MPs. The entirety of the FIS setup was assembled on top of a height-adjustable table. The sCMOS region of interest was between x = 3.65 m and x = 3.85 m of the experimental flume.

The FIS was calibrated on an isolated 10 cm section of the flume, which was filled with MPs suspensions and MPs in the pore space of the sediment. This allowed for the calculation of two separate calibration lines, one for the water area and one for the sediment area of the camera's field of view. The pixel values of the calibration area were then averaged to produce a calibration line. This pixel data was further refined by removing the values that fell beyond 3σ of the mean value. The LOD and LOQ were calculated from the calibration curves described above. To better illuminate the calibration area, the height of the table was adjusted so that the center of the laser illuminated area would be within the calibration region of interest.

To determine the area illuminated by the laser, we used a purpose-built 60 × 30 × 5 cm glass tank positioned inside the flume. This tank was then filled with DI water and spiked with different concentrations of compounds, and the height of the table was set to the same height

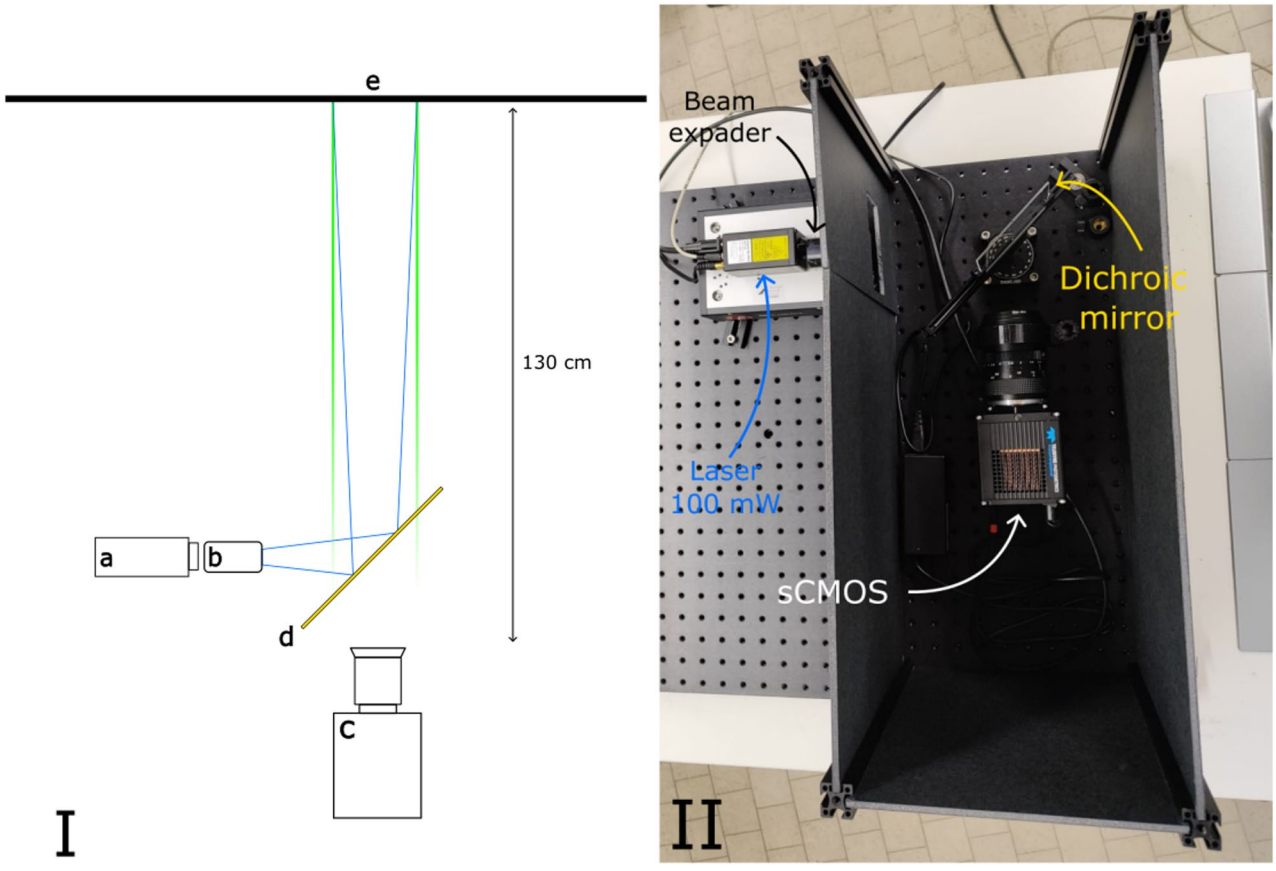


**Fig. 3** Schematics and image of the FIS system. Ia) 457 nm 100 mW laser, Ib) 40x beam expander, Ic) sCMOS camera, Id) dichroic mirror, Ie) flume wall. The FIS system was placed 130 cm from the flume wall, and the whole FIS setup was encased in an optical enclosure mounted on an aluminum breadboard. II shows the FIS setup with the top of the optical enclosure removed

used during the experiments. This allowed us to find the areas consistently illuminated at various concentrations, and to generate a circular mask centered on the center of illumination and radius equal to the Euclidean distance from the center to the illumination's edge.

To minimize changes in the setup, the FIS was not moved between calibrations, and the height of the table was maintained the same as during the determination of the illumination area. After injecting the compound of interest in the flume, we recorded with the FIS at eight frames per second for 30 min with an exposure time of 100ms. To process the data, the first ten images taken by the FIS were averaged, and the resulting averaged image was subtracted from all the other images to act as a blank and to remove the signal coming from the sediment. Each image taken within a second was averaged to reduce noise and obtain a representative signal. This was done every ten seconds to produce a single image representative of the concentration within the study area, thus having an image every ten seconds of the experiment. This resulted in one average frame for every 10 s of recording. These images were then processed by multiplying the sedimented and water areas for the respective calibration curve to obtain the concentration of fluorescent compound for each image. Since a higher concentration was used during the IMPs experiment, the results show a higher background. To minimize the impact of this high background during the determination of the infiltration depths of IMPs, the images were preprocessed by applying Contrast Limited Adaptive Histogram Equalization (CLAHE), image normalization, and Gaussian blurring on all the images. This proved necessary as the IMPs had a lower response to our detection devices compared to other particle types used in the experiments.

To measure the particles' infiltration depths, the average frame every 5 min of the experiment was preprocessed by applying a Gaussian blur and CLAHE, and its center of mass was tracked on the vertical y-axis. From the determined y-position in time infiltration depth, the infiltration velocity was calculated as

$$v_i = \frac{y_t - y_{t-\Delta t}}{\Delta t} \tag{3}$$

Where $y_t$ [L] is the location of the center of mass y value at time t, and $t_i$ is the time at index i. To obtain a representative depth for each infiltration velocity, the corresponding depth for each velocity was calculated as

$$d_i = \frac{y_t - y_{t-\Delta t}}{2} \tag{4}$$

Where $d_i$ is the average depth between two $y_i$ measurements.

Furthermore, to allow for the comparison between experiments, the NMT for all FIS results was calculated by using Eq. 1. We performed all the data processing and the calculations using various Python libraries.

## Results

### Particle breakthrough and retention

Figure 4 shows the data obtained from the fluorometers installed at points x = 2.40 m (inflow) and x = 4.90 m (outflow) of the flume. Figure 4a shows the NMT observed at the outflow fluorometer, with all the compounds reaching the fluorometers at similar times. To better compare the arrival of the different compounds, peak arrival time was defined as the time at which the highest NMT was detected from the injection of each compound. Peak arrival is delayed for the IMPs and MPFs compared to the SMPs and fluorescein. Fluorescein and SMPs peak arrival time is almost identical (Table 2). Peak concentration arrival height is comparable for IMPs and MPFs, with peak height being higher for the SMPs than the other two types (1.2% higher compared to the MPFs, and 2.4% higher compared to the IMPs). Peak NMT for fluorescein is also higher than the other compounds (7% for the IMPs, 8% for the MPFs, and 7% for the SMPs). NMTs for the IMPs and MPFs decrease more slowly in the falling limb than for the 10 μm SMPs, indicating a longer residence time in the monitoring section of the flume. NMTs detection limit (indicated by the dashed lines in Fig. 4a) was similar for each compound, with fluorescein having the highest detection limit of the fluorescent compounds (SI). This was due to the low concentration used during the experiment. Such low concentration was necessary to ensure that the signal for the FIS system remained within the measurable range. The initial concentrations for the IMPs and MPFs are above the detection limit. This is due to the large number of particles used during the experiments and calibrations, which were necessary to have a high enough signal to be detected by our devices. While this could lead to overestimating the concentration of IMPs and MPFs at low concentrations, each measurement before the compounds' introduction constitutes less than 0.02% of the introduced mass. Thus, we consider the error this overestimation produces as inconsequential for our results.

To better compare the retention times of each compound, we calculated the time difference between when the result of Eq. 2 goes from ≈ 100% to less than 5%. The retention of IMPs in the studied flume section was comparable to that of SMPs. Particles were flushed from the system, with 95% of the introduced mass being removed after 304 s for SMPs and 414 s for IMPs. As evidenced by the difference in MPs' residence time, the IMPs are stored in the study area longer than the SMPs. Fluorescein was flushed from the system most rapidly, with 95%

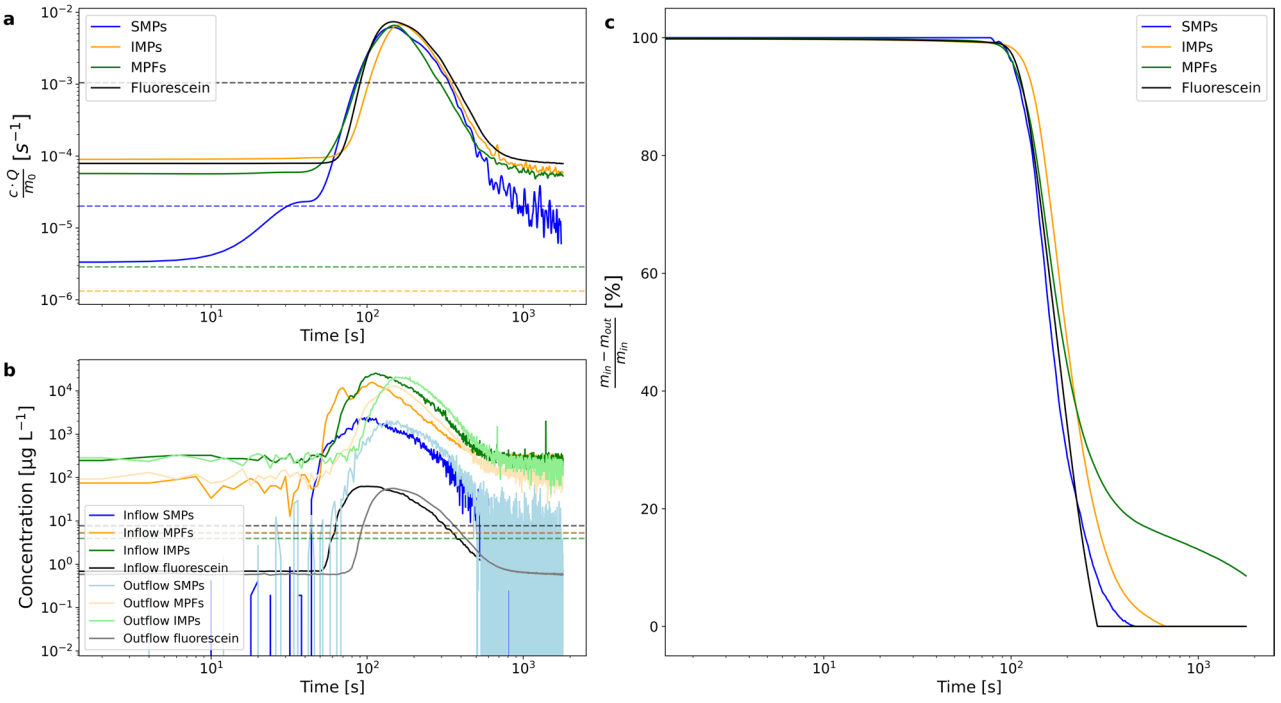


**Fig. 4** Results of the outflow concentration measurements. (**a**) Normalized mass transfer of MPs was measured using the outflow fluorometer, displayed using a logarithmic scale. Dashed lines represent the LOD of each measurement. Normalization was achieved using Eq. 1; (**b**) concentration of MPs as detected from both the inflow and outflow fluorometer displayed using a logarithmic scale. Dashed lines represent the LOD of each measurement; (**c**) stored MPs mass in the study area throughout the experiment. The data was obtained by using Eq. 2

**Table 2** Peak arrival times and retention times for each fluorescent compound. The retention time value for MPFs is missing, as the value never dropped below 5%; thus, the percentage of retained particles is given instead

| | SMPs | IMPs | MPFs | Fluorescein |
|---|---|---|---|---|
| Peak arrival time [s] | 146 | 164 | 150 | 148 |
| Retention time [s] | 304 | 414 | *9% left* | 268 |

of the introduced tracer exiting after 268 s. For MPFs, only 91% of the introduced mass was flushed from the system by the end of the experiment, indicating higher retention of fibers in the monitored section compared to IMPs and SMPs. Whether the retention for MPFs was temporary or permanent could not be determined during the experiments.

### Infiltration dynamics and sediment penetration depths

FIS images (Fig. 5) illustrate the infiltration patterns of the different particles on the stoss side of the monitored ripple. SMPs infiltrate into the sediment and distribute within the pore space, spanning from the infiltration point on the stoss side to the maximum depth reached by the end of the experiment, as previously also reported by Boos et al. [41]. This behavior is not observed for the other particle types, which maintain a contiguous cloud-like structure during infiltration. Furthermore, no particles remain trapped between the sediment crest and the particle cloud. Particle infiltration of IMPs, MPFs, and fluorescein exhibits a similar behavior, characterized by a distinct lenticular breakthrough pattern within the sediment. MPFs seem to accumulate at the sediment–water interface preferentially on the stoss side of the monitored ripple, as indicated by a strong fluorescent signal persisting at the top of the stoss side at the end of the experiment (a video showing this kind of behavior is presented as part of the supplement S1).

Penetration depths and infiltration velocities for the different MPs are shown in Fig. 6. Figure 6b shows that the timescale of infiltration into the ripple is similar for all compounds, meaning that infiltration begins similarly for all compounds and reaches the highest infiltration depth by the end of the experiment. However, the maximum infiltration depth after 1500 s varies between them (Table 3). Maximum infiltration depth is the lowest for the 10 µm SMPs, with a depth of 8 cm below the crest, and highest for the 1 µm SMPs, with 12 cm. The penetration depths of MPFs were similar to those of the 3 µm SMPs, both reaching approximately 10 cm below the crest, while the IMPs reached a depth of 9 cm below the crest. Average infiltration velocities were estimated from the fitted trendline. These averages were comparable across the different particle types, with SMPs exhibiting the highest average velocity (approximately 0.22 mm $s^{-1}$), while fluorescein SMPs had the lowest average velocity

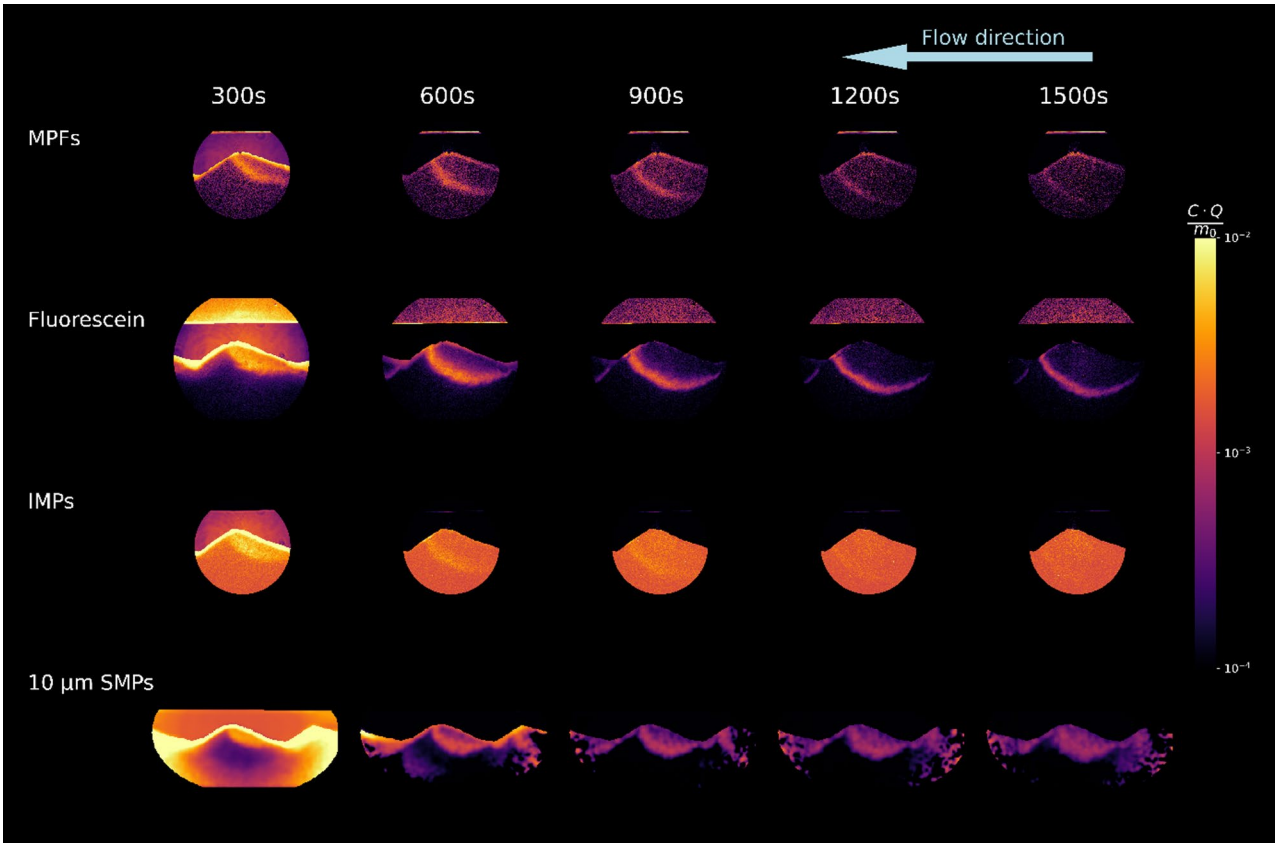


**Fig. 5** Calibrated results from the FIS system for the 10 µm MPs (Spheres), IMPs (Fragments), MPFs (Fibers), and Fluorescein. The results for the 10 µm MPs are adapted from Boos et al. [41]. While the setup used was comparable to the one used here, the sCMOS and the laser used here were different from those used by Boos et al. To make the comparison between results easier, we normalized the calibrated images by using Eq. 2

(around 0.10 mm $s^{-1}$). All calculated infiltration average velocities are listed in Table 3. Infiltration velocities approximately decreased exponentially with depth, as shown in Fig. 6c.

## Discussion

Each particle type exhibited distinct transport behavior throughout the experiments, highlighting particle-specific transport characteristics. The fluorescein tracer and the 10 µm SMPs had the earliest peak arrival time. Fluorescein's total residence time within the study section was the shortest, as the dye was rapidly flushed from the system. Except for the fibers, all tested particles showed minimal retention within the flume's study section, with nearly 100% of the applied mass being flushed out by the end of the experiment. Irregularly shaped MPs demonstrated slightly longer residence times in the streambed sediments compared to fluorescein and SMPs. However, their overall transport behavior closely resembled that of the spherical particles. Longer residence times of irregular particles relative to spherical ones (414 s vs. 304 s) may be explained by increased particle-sediment interactions, likely due to the rougher surfaces and more complex geometries of the irregular fragments compared to the smooth spheres used in our experiments.

MPFs were the only particle type used in the experiments that were not entirely flushed from the study section by the end of the experiment. This suggests that fibrous particles exhibit the highest retention compared to spherical or irregularly shaped particles. FIS images indicated that retention occurred within the streambed sediments and at the streambed-water interface. This difference in behavior can be better understood by considering the varying size ratios between the MPs and the sediment particles. By considering the particle size to sediment size ratio in Table 1, the infiltration depth of the different particles followed their particle-to-sediment size ratio, with smaller ratios resulting in deeper infiltration into the streambed. In comparison, larger ratios led to shallower penetration depths. This ratio has been used as a reliable indicator for MPs' sediment penetration in column infiltration experiments [33]. While this ratio doesn't reliably measure the infiltration capability of MPs outside of column experiments, it can be used to compare the infiltration of the IMPs and MPFs to the SMPs present in the literature. As opposed to the SMPs and IMPs, the mobility of MPFs can be explained by

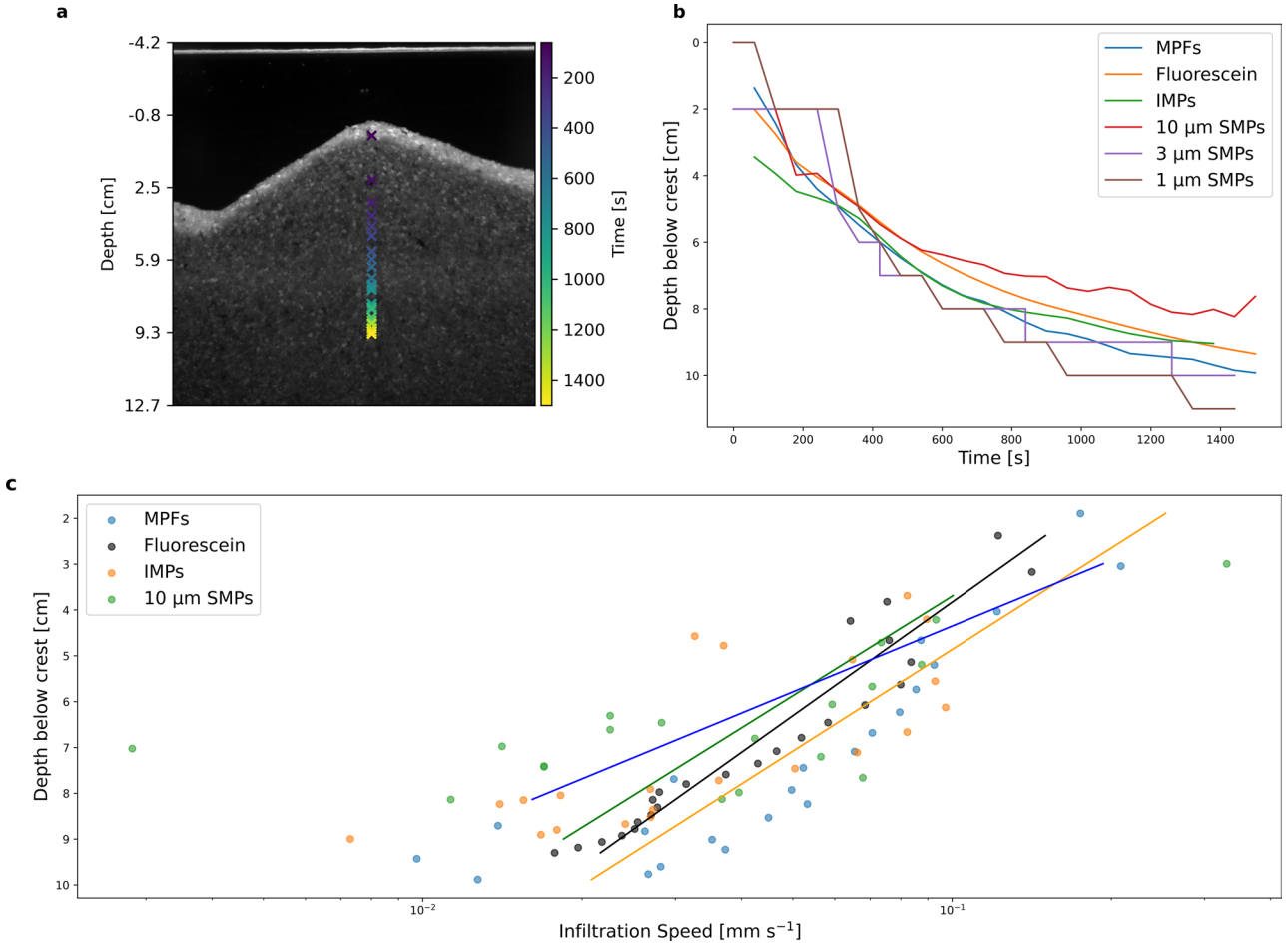


**Fig. 6** (**a**) Example image of the results from the depth detection logic used to detect the depth of the infiltrated MPs. These results from the MPFs experiment, plotted on top of the sediment dune, show how deep the particles reach within the dune with MPFs as an example. (**b**) Infiltration depth reached by each fluorescent compound within the sediment. (**c**) Infiltration velocity of each fluorescent compound. Note that the x-axis is plotted using a logarithmic scale. The trendline was calculated as the logarithmic regression of each dataset plotted. The equations are in Table 3. The datasets of the 10 µm MPs, 3 µm MPs, and 1 µm MPs were adapted from Boos et al. [46]

**Table 3** Maximum infiltration depths reached at t = 1500s, average velocity for each compound where it was possible to calculate it, and the fitted regression line equations

| Compound | MPFs | Fluorescein | IMPs | 10 µm SMPs | 3 µm SMPs | 1 µm SMPs |
|---|---|---|---|---|---|---|
| Final Depth [cm] | 10 | 9 | 9 | 8 | 10 | 11 |
| Average infiltration velocity [mm s$^{-1}$] | 0.14 | 0.10 | 0.11 | 0.22 | - | - |
| Fitted regression line equation (log(v) = a·d + b) | log(v)= -0.31 ·d-0.78 | log(v)= -0.28 ·d-1.23 | log(v)= -0.32 ·d-1.12 | log(v)= -0.48 ·d-0.20 | - | - |

considering their particle-to-sediment size ratio in two dimensions: one based on their diameter and the other on their length.

The maximum infiltration depth of MPFs into the sediment is similar to that of the 3 µm SMPs, consistent with the particle-to-sediment size ratio based on diameter. However, FIS images revealed that a substantial fraction of the fibers accumulated at the sediment–water interface. This suggests that their penetration into the sediment was likely inhibited by their length and the transport orientation, which prevented entry into the pore spaces. This accumulation of MPFs on the surface of the sediment has already been found in previous laboratory experiments [47]. MPFs that failed to infiltrate into the sediments likely approached the stoss side of the dune at suboptimal incidence angles, causing them to settle on the sediment surface. In contrast, MPFs arriving at more favorable angles were able to penetrate the sediment, reaching infiltration depths comparable to those observed for similarly sized spherical microplastics. Findings from previous studies support the idea that the three-dimensional nature of the MPFs can hinder

infiltration, as they have to be aligned with the sediment's pore space to be able to infiltrate [48]. Although we did not directly test this, we believe that the fibers retained at the sediment–water interface represent a substantial fraction of the remaining fibers at the end of the experiment.

The preferential retention of fibers at the streambed–sediment interface represents a behavior not previously reported in the literature. This indicates that, in addition to the sediments, the streambed-water interface also serves as a preferential accumulation zone for fibrous particles. High concentrations of fibers have been reported in streambed sediments across a wide range of river and stream systems globally [49, 50]. Fibers have been found in the digestive tracts of freshwater organisms, particularly those living in the sediments or grazing near the sediment-water interface [51]. Such ingestion can lead to an increased organism mortality and the transfer of MPs to higher trophic levels within the food web [52]. Compared to other particle shapes, the longer retention times of fibers at the streambed-water interface may lead to prolonged environmental exposure and a heightened risk of uptake by benthic and benthopelagic organisms. Since entry into food webs often occurs via benthic organisms, understanding the transport and retention behavior of pore-scale MPFs and irregular IMPs is a crucial area of research.

The sediment ripple configuration was kept consistent throughout our research to ensure comparability, but such stability is unrealistic compared to real riverine systems. The hydrodynamic process that happens in nature, such as in rivers and streams, naturally forms structures like those used in our research, but these structures are generally unstable and subject to change. Such structures are susceptible to discharge and water temperature changes [53], variables that were kept as constant as possible during our experiments. Such instability is essential for the study of the MPs' infiltration mechanisms, as the sedimentation cycle of a river bed could entrap suspended MPs [54] or remobilize already buried MPs [55]. The sedimentation cycle could be one of the pathways larger MPFs take to infiltrate deeper in the sediment bed. Since MPFs accumulated on the stoss side of the ripples, subsequent sediment deposition driven by water flow could bury these MPFs, leading to their retention in the sediment bed despite their inability to infiltrate advectively. In real-world conditions, flooding has been reported to significantly impact the MPs' concentration in the sediment and water. Flooding events are connected to an increase in the MPs concentration in the surface water [56], while in the sediment, the concentration can either increase or decrease [57, 58]. Additionally, the flow velocity used in our research is representative only of small streams [59, 60], whereas larger rivers tend to have much greater water velocities [61, 62]. These greater velocities will likely decrease the residence time of the particles within the sediment, and they would be that of a transitional or turbulent regime. Since rivers typically have a turbulent regime [63], higher flow velocities and Reynolds number conditions need to be tested to better understand the transport of MPs in realistic environments. Because of the limited timescale and discharge used for the experiments conducted here, the impact of dynamic flow on the MPs concentration and their infiltration potential could not be investigated. Furthermore, a timescale of 30 min, such as the one used in our experiments, is not representative of environmental conditions, where the residence time of rivers is much larger [64, 65]. While our results give an insight into the effect of shape on the infiltration potential of MPs in a sediment bed, the impact that the instability of riverbeds and a dynamic flow have on MPs' infiltration is an area that needs more research. Additionally, longer experimental exposure of the sediment to MPs and water would be necessary to investigate the prolonged exposure of riverbeds to deposited and infiltrated MPs.

Although the particles used in our experiments resemble environmentally relevant shapes, they were pristine and had not been exposed to natural environmental conditions prior to flume testing. MPs in the environment are subject to UV and mechanical weathering [66, 67]. This weathering process can produce smaller MPs and change the surface properties of the MPs [68]. Furthermore, MPs in environmental conditions form "Eco-coronas", an outer layer of adsorbed compounds that change the surface properties of the MPs [69]. Such a change in the surface properties has been linked to enhanced interactions with microorganisms, aiding their phagocytosis [70] and increasing their exposure to toxic compounds [71]. As such, the effects that a realistic eco-corona would have on MPS's transport and infiltration capacity were not investigated.

## Conclusions

This study provides a mechanistic comparison of the mobility and retention of spherical, irregular, and fibrous microplastics in an idealized stream and its streambed sediments. Fibrous MPs were found to infiltrate into the sediment similarly to spherical MPs of comparable diameter, but only if their impact angle allows the fiber to enter the sediment from its circular cross-section. Suboptimal impact angles result in fibers settling on the sediment surface, from which they are slowly released. This surface settling, followed by burial under accumulating sediments, may explain how fibers too large to penetrate riverine sediment pores are nonetheless found at depth. Irregular MPs, in contrast, infiltrate the hyporheic zone similarly to spherical MPs with a comparable hydraulic

diameter, but they exhibit longer retention within the sediment. These results indicate that MP shape strongly influences sediment interaction. The extended residence time, especially for fibrous MPs, increases their potential interactions with benthic organisms.

**Abbreviations**

| | |
|---|---|
| MPs | Microplastics |
| SMPs | Spherical microplastics |
| IMPs | Irregular microplastics |
| MPFs | Microplastic fibers |
| DI water | Deionized water |
| PIV | Particle image velocimetry |
| PS | Polystyrene |
| PET | Polyethylene terephthalate |
| LOD | Limit of detection |
| LOQ | Limit of quantification |
| FIS | Fluorescence imaging system |
| NMT | Normalized mass transfer |

## Supplementary Information

The online version contains supplementary material available at https://doi.org/10.1186/s43591-025-00165-2.

Supplementary Material 1

Supplementary Material 2

**Acknowledgements**
The authors would like to express their gratitude to Martina Rohr, Markus Scholz, and Isolde Baumann for their invaluable technical support during the laboratory experiments.

**Author contributions**
MLC carried out the experiments. DW manufactured the microplastics used in the experiments. MLC wrote the manuscript with support from SF, JHF, DW, and SA. SF conceived the project and supervised it. All authors reviewed the manuscript.

**Funding**
Open Access funding enabled and organized by Projekt DEAL. This project was funded by the Deutsche Forschungsgemeinschaft (DFG, German Research Foundation)—Project Number 391977956—SFB 1357.

**Data availability**
The datasets generated and analyzed during the current study are available in the Zenodo repository, https://doi.org/10.5281/zenodo.17249162. Raw images can be obtained from the authors upon reasonable request.

## Declarations

**Competing interests**
The authors declare no competing interests.

**Author details**
[1]Department of Hydrology, Bayreuth Center of Ecology and Environmental Research (BayCEER), University of Bayreuth, Bayreuth, Germany
[2]Advanced Sustainable Polymers, Macromolecular Chemistry II, University of Bayreuth, Bayreuth, Germany
[3]Department of Hydrogeology, Helmholtz-Centre for Environmental Research, UFZ, Leipzig, Germany
[4]Hydrologic Modelling Unit, Bayreuth Center of Ecology and Environmental Research (BayCEER), University of Bayreuth, Bayreuth, Germany
[5]Department of Aquatic Ecology and Water Quality Management, Wageningen University & Research, Wageningen, Netherlands

Received: 10 October 2025 / Accepted: 1 December 2025
Published online: 26 December 2025

**References**

1. Sorensen RM, Jovanović B. From nanoplastic to microplastic: a bibliometric analysis on the presence of plastic particles in the environment. Mar Pollut Bull. 2021;163:111926.
2. UNEP. Frontiers 2017 emerging issues of environmental concern. Nairobi: United Nations Environment Programme; 2017.
3. Chia RW, Lee JY, Kim H, Jang J. Microplastic pollution in soil and groundwater: a review. Environ Chem Lett. 2021;19(6):4211–24.
4. Ivar Do Sul JA, Costa MF. The present and future of microplastic pollution in the marine environment. Environ Pollut. 2014;185:352–64.
5. Li C, Busquets R, Campos LC. Assessment of microplastics in freshwater systems: A review. Sci Total Environ. 2020;707:135578.
6. Xu B, Liu F, Cryder Z, Huang D, Lu Z, He Y, et al. Microplastics in the soil environment: Occurrence, risks, interactions and fate – A review. Crit Rev Environ Sci Technol. 2020;50(21):2175–222.
7. Peng X, Chen M, Chen S, Dasgupta S, Xu H, Ta K, et al. Microplastics contaminate the deepest part of the world's ocean. Geochem Perspect Lett. 2018;1–5.
8. De Souza Machado AA, Lau CW, Till J, Kloas W, Lehmann A, Becker R, et al. Impacts of microplastics on the soil biophysical environment. Environ Sci Technol. 2018 Sept 4;52(17):9656–65.
9. Zhang X, Li Y, Ouyang D, Lei J, Tan Q, Xie L, et al. Systematical review of interactions between microplastics and microorganisms in the soil environment. J Hazard Mater. 2021 Sept 15;418:126288.
10. Zhao B, Rehati P, Yang Z, Cai Z, Guo C, Li Y. The potential toxicity of microplastics on human health. Sci Total Environ. 2024;912:168946.
11. Danopoulos E, Twiddy M, Rotchell JM. Microplastic contamination of drinking water: a systematic review. Plos ONE 2020 July 31;15(7):e0236838.
12. Kwon JH, Kim JW, Pham TD, Tarafdar A, Hong S, Chun SH, et al. Microplastics in food: A review on analytical methods and challenges. Int J Environ Res Public Health. 2020;17(18):6710.
13. Baldwin AK, Corsi SR, Mason SA. Plastic debris in 29 great lakes tributaries: relations to watershed attributes and hydrology. Environ Sci Technol. 2016;50(19):10377–85.
14. Brewer A, Dror I, Berkowitz B. The mobility of plastic nanoparticles in aqueous and soil environments: A critical review. ACS EST Water. 2021;1(1):48–57.
15. Mani T, Primpke S, Lorenz C, Gerdts G, Burkhardt-Holm P. Microplastic pollution in benthic midstream sediments of the rhine river. Environ Sci Technol. 2019;53(10):6053–62.
16. Mao Y, Li H, Gu W, Yang G, Liu Y, He Q. Distribution and characteristics of microplastics in the Yulin River, china: role of environmental and Spatial factors. Environ Pollut. 2020;265:115033.
17. Zhang D, Liu X, Huang W, Li J, Wang C, Zhang D, et al. Microplastic pollution in deep-sea sediments and organisms of the Western Pacific ocean. Environ Pollut. 2020;259:113948.
18. Horton AA, Dixon SJ. Microplastics: an introduction to environmental transport processes. WIREs Water. 2018;5(2):e1268.
19. Frei S, Piehl S, Gilfedder BS, Löder MGJ, Krutzke J, Wilhelm L, et al. Occurence of microplastics in the hyporheic zone of rivers. Sci Rep. 2019;9(1):15256.
20. Xia F, Tan Q, Qin H, Wang D, Cai Y, Zhang J. Sequestration and export of microplastics in urban river sediments. Environ Int. 2023;181:108265.
21. Lenaker PL, Baldwin AK, Corsi SR, Mason SA, Reneau PC, Scott JW. Vertical distribution of microplastics in the water column and surficial sediment from the Milwaukee river basin to lake Michigan. Environ Sci Technol. 2019;53(21):12227–37.
22. Pasquier G, Doyen P, Dehaut A, Veillet G, Duflos G, Amara R. Vertical distribution of microplastics in a river water column using an innovative sampling method. Environ Monit Assess. 2023;195(11):1302.
23. Niu L, Wang Y, Li Y, Lin L, Chen Y, Shen J, Occurrence. Degradation pathways, and potential synergistic degradation mechanism of microplastics in surface water: a review. Curr Pollut Rep. 2023 June 1;9(2):312–26.
24. Sooriyakumar P, Bolan N, Kumar M, Singh L, Yu Y, Li Y, et al. Biofilm formation and its implications on the properties and fate of microplastics in aquatic environments: A review. J Hazard Mater Adv. 2022;6:100077.
25. Yan M, Wang L, Dai Y, Sun H, Liu C. Behavior of microplastics in inland waters: Aggregation, Settlement, and transport. Bull Environ Contam Toxicol. 2021;107(4):700–9.

26. Dittmar S, Ruhl AS, Altmann K, Jekel M. Settling velocities of small microplastic fragments and fibers. Environ Sci Technol. 2024;58(14):6359–69.
27. Mancini M, Serra T, Colomer J, Solari L. Suspended sediments mediate microplastic sedimentation in unidirectional flows. Sci Total Environ. 2023 Sept 10;890:164363.
28. Pohl F, Eggenhuisen JT, Kane IA, Clare MA. Transport and burial of microplastics in Deep-Marine sediments by turbidity currents. Environ Sci Technol. 2020;54(7):4180–9.
29. Hurley R, Woodward J, Rothwell JJ. Microplastic contamination of river beds significantly reduced by catchment-wide flooding. Nat Geosci. 2018;11:251–7.
30. Koelmans AA, Hasselerharm PER, Nor NHM, de Ruijter VN, Mintenig SM, Kooi M. Risk assessment of microplastic particles. Nat Rev Mater. 2022;7(2):138–52.
31. Sun Y, Duan C, Cao N, Li X, Li X, Chen Y, et al. Effects of microplastics on soil microbiome: the impacts of polymer type, shape, and concentration. Sci Total Environ. 2022;806:150516.
32. Waldschläger K, Schüttrumpf H. Erosion behavior of different microplastic particles in comparison to natural sediments. Environ Sci Technol. 2019;53(22):13219–27.
33. Waldschläger K, Schüttrumpf H. Infiltration behavior of microplastic particles with different Densities, Sizes, and Shapes—From glass spheres to natural sediments. Environ Sci Technol. 2020;54(15):9366–73.
34. Boos JP, Gilfedder BS, Frei S. Tracking microplastics across the streambed interface: using Laser-Induced-Fluorescence to quantitatively analyze microplastic transport in an experimental flume. Water Resour Res. 2021;57(12):e2021WR031064.
35. Dichgans F, Boos JP, Ahmadi P, Frei S, Fleckenstein JH. Integrated numerical modeling to quantify transport and fate of microplastics in the hyporheic zone. Water Res. 2023 Sept;1:243:120349.
36. Rozman U, Kalčíková G. Seeking for a perfect (non-spherical) microplastic particle – The most comprehensive review on microplastic laboratory research. J Hazard Mater. 2022;424:127529.
37. Akdogan Z, Guven B, Kideys AE. Microplastic distribution in the surface water and sediment of the ergene river. Environ Res. 2023;234:116500.
38. Bonyadi Z, Maghsodian Z, Zahmatkesh M, Nasiriara J, Ramavandi B. Investigation of microplastic pollution in Torghabeh river sediments, Northeast of Iran. J Contam Hydrol. 2022;250:104064.
39. Li Y, Lu Q, Yang J, Xing Y, Ling W, Liu K, et al. The fate of microplastic pollution in the Changjiang river estuary: A review. J Clean Prod. 2023;425:138970.
40. Fox A, Boano F, Arnon S. Impact of losing and gaining streamflow conditions on hyporheic exchange fluxes induced by dune-shaped bed forms. Water Resour Res. 2014;50(3):1895–907.
41. Boos JP, Dichgans F, Fleckenstein JH, Gilfedder BS, Frei S. Assessing the behavior of microplastics in fluvial systems: infiltration and retention dynamics in streambed sediments. Water Resour Res. 2024;60(2):e2023WR035532.
42. Agarwal S, Burgard M, Greiner A, Wendorff J, Electrospinning. A practical guide to nanofibers. Walter de Gruyter GmbH & Co KG; 2016. p. 190.
43. Jiang S, Greiner A, Agarwal S. Short nylon-6 nanofiber reinforced transparent and high modulus thermoplastic polymeric composites. Compos Sci Technol. 2013;87:164–9.
44. Thieme M, Agarwal S, Wendorff JH, Greiner A. Electrospinning and cutting of ultrafine bioerodible poly(lactide-co-ethylene oxide) tri- and multiblock copolymer fibers for inhalation applications. Polym Adv Technol. 2011;22(9):1335–44.
45. Schnegg PA. An inexpensive field fluorometer for hydrogeological tracer tests with three tracers and turbidity measurement. Groundwater and Human Development; 2002. p. 6.
46. Boos JP, Dichgans F, Fleckenstein JH, Gilfedder B, Frei S. Data and code for the publication assessing the behavior of microplastics in fluvial systems: infiltration and retention dynamics in streambed sediments - Part 1(2) [Internet]. Zenodo; 2023 [cited 2025 July 8]. Available from: https://zenodo.org/records/10083568
47. Mancini M, Francalanci S, Innocenti L, Solari L. Investigations on microplastic infiltration within natural riverbed sediments. Sci Total Environ. 2023;904:167256.
48. Qiao X, Qian S, Dong S, Zhu DZ, Feng J, Xu H, et al. Real-Time visualization of infiltration and retention of microplastics with different shapes in porous media. Environ Sci Technol. 2024;58(47):21037–45.
49. Horton AA, Svendsen C, Williams RJ, Spurgeon DJ, Lahive E. Large microplastic particles in sediments of tributaries of the river Thames, UK – Abundance, sources and methods for effective quantification. Mar Pollut Bull. 2017;114(1):218–26.
50. Liu R ping, Li Z zhong, Liu F, Dong Y, Jiao J gang, Sun P ping, et al. Microplastic pollution in yellow river, China: current status and research progress of biotoxicological effects. China Geol. 2021;4(4):585–92.
51. Albarano L, Maggio C, La Marca A, Iovine R, Lofrano G, Guida M, et al. Risk assessment of natural and synthetic fibers in aquatic environment: a critical review. Sci Total Environ. 2024 July;15:934:173398.
52. Rebelein A, Int-Veen I, Kammann U, Scharsack JP. Microplastic fibers — Underestimated threat to aquatic organisms? Sci Total Environ. 2021 July 10;777:146045.
53. Southard JB. Experimental determination of Bed-Form stability. Annu Rev Earth Planet Sci. 1991;19:423–55.
54. Beaumont H, Ockelford A, Morris-Simpson P. Sand bed river dynamics controlling microplastic flux. Sci Rep. 2024;14(1):29420.
55. Peleg E, Teitelbaum Y, Arnon S. Exploring the influence of sediment motion on microplastic deposition in streambeds. Water Res. 2024;249:120952.
56. Patterson J, Jeyasanta KI, Sathish MN, Booth AM, Laju RL, Emeralda VG, et al. Impact of flooding events on microplastic distribution from rivers to coastal areas: a case study from Tuticorin, Southeast India. Mar Pollut Bull. 2025;221:118471.
57. Eppehimer DE, Hamdhani H, Hollien KD, Nemec ZC, Lee LN, Quanrud DM, et al. Impacts of baseflow and flooding on microplastic pollution in an effluent-dependent arid land river in the USA. Environ Sci Pollut Res. 2021 Sept 1;28(33):45375–89.
58. Lahon J, Handique S. Impact of flooding on microplastic abundance and distribution in freshwater environment: a review. Environ Sci Pollut Res. 2023;30(56):118175–91.
59. Bradley AA, Kruger A, Meselhe EA, Muste MVI. Flow measurement in streams using video imagery. Water Resour Res. 2002;38(12):51–1.
60. Waldon MG. Estimation of average stream velocity. J Hydraul Eng. 2004;130(11):1119–22.
61. Verzano K, Bärlund I, Flörke M, Lehner B, Kynast E, Voß F, et al. Modeling variable river flow velocity on continental scale: current situation and climate change impacts in Europe. J Hydrol. 2012;424–425:238–51.
62. Nittrouer JA, Shaw J, Lamb MP, Mohrig D. Spatial and Temporal trends for water-flow velocity and bed-material sediment transport in the lower Mississippi river. GSA Bull. 2012;124(3–4):400–14.
63. FrancaMJ, Brocchini M. Turbulence in Rivers. In: Rowiński P, Radecki-Pawlik A, editors. Rivers – physical, fluvial and environmental processes [Internet]. Cham: Springer International Publishing; 2015 [cited 2025 Nov 12]. pp. 51–78. Available from: https://doi.org/10.1007/978-3-319-17719-9_2.
64. Kralik M, Humer F, Fank J, Harum T, Klammler G, Gooddy D, et al. Using 18O/2H, 3H/3He, 85Kr and CFCs to determine mean residence times and water origin in the grazer and Leibnitzer feld groundwater bodies (Austria). Appl Geochem. 2014;50:150–63.
65. Chen M, Xing N, Huang Y, Qiu Y. The mean residence time of river water in the Canada basin. Chin Sci Bull. 2008;53(5):777–83.
66. Ameen A, Stevenson ME, Kirschner AKT, Jakwerth S, Derx J, Blaschke AP. Fate and transport of fragmented and spherical microplastics in saturated gravel and quartz sand. J Environ Qual. 2024;53(5):727–42.
67. Pinlova B, Nowack B. From cracks to secondary microplastics - surface characterization of polyethylene terephthalate (PET) during weathering. Chemosphere. 2024;352:141305.
68. Schmidtmann J, Weishäupl HK, Hopp L, Meides N, Peiffer S. UV-weathering affects heteroaggregation and subsequent sedimentation of polystyrene microplastic particles with ferrihydrite. Environ Sci Process Impacts. 2025;27(4):992–1002.
69. Zhang P, Liu Y, Zhang L, Xu M, Gao L, Zhao B. The interaction of micro/nano plastics and the environment: effects of ecological Corona on the toxicity to aquatic organisms. Ecotoxicol Environ Saf. 2022 Sept 15;243:113997.
70. Ramsperger AFRM, Narayana VKB, Gross W, Mohanraj J, Thelakkat M, Greiner A, et al. Environmental exposure enhances the internalization of microplastic particles into cells. Sci Adv. 2020;6(50):eabd1211.
71. Sundar Sarmila A, Chandrasekaran N. Prepared polypropylene microplastics: formation of eco-corona in aquatic systems and their combined toxicity with cadmium in Artemia franciscana. Environ Sci Process Impacts [Internet]. 2025 [cited 2025 Sept 3]; Available from: https://pubs.rsc.org/en/content/articlelanding/2025/em/d5em00260e.


## Publisher's note